Am J Cancer Res 2023;13(7):3234-3245
www.ajcr.us /ISSN:2156-6976/ajcr0151201

Original Article

Calcium dobesilate prevents PLD-induced hand-foot syndrome by alleviating capillary endothelial tight junction injury via the HA/CD44 pathway

Chao Li[1], Bin Xu[1], Heng Song[1], Yu Xu[1], Ling-Zi Shi[1], Xiao-Qing Chen[1], Zhen-Chuan Song[1,2]

[1]Department of Breast Center, The Fourth Hospital of Hebei Medical University, Shijiazhuang 050000, Hebei, P. R. China; [2]Key Laboratory for Breast Cancer Molecular Medicine of Hebei Province, Shijiazhuang 050000, Hebei, P. R. China

Received May 12, 2023; Accepted July 12, 2023; Epub July 15, 2023; Published July 30, 2023

Abstract: Pegylated liposomal doxorubicin (PLD) has excellent therapeutic efficacy in the treatment of cancers, but can cause serious adverse reactions such as hand-foot syndrome (HFS). Our previous research suggests that both PLD-induced HFS may be associated with injury to tight junctions (TJs) in the skin and that calcium dobesilate (CaD) can alleviate HFS. However, the underlying molecular mechanism is not well understood. Here, we created an in vitro PLD-treated model using Human Microvascular Endothelial Cell line-1 (HMEC-1) and an in vivo HFS rat model to investigate the underlying pathways. Treatment with PLD increased the expression of HYAL-1, CD44, and hyaluronic acid (HA) concentration, while reducing ZO-1 and Claudin-5 expression. Moreover, PLD treatment induced the degradation of higher molecular weight HA to its lower molecular weight counterpart, elevating the permeability of both HEMC-1 cell membranes and rat paw skin capillaries. AD-01 (CD44 inhibitor) inhibited the effect of PLD on the expression of ZO-1 and Claudin-5. Furthermore, CaD treatment suppressed the expression of HYAL-1 and CD44, mitigated HA degradation, and enhanced the expression of ZO-1 and Claudin-5. This resulted in decreased permeability in HEMC-1 cells and rat skin capillaries. In summary, our data suggest that PLD may promote the destruction of TJs via the HA/CD44 pathway, thereby leading to HFS through increased skin permeability and exacerbated doxorubicin extravasation. Moreover, CaD can inhibit this pathway, offering a potential therapeutic avenue to alleviate HFS.

Keywords: Pegylated liposomal doxorubicin, hand-foot syndrome, hyaluronic acid/CD44 pathway, tight junctions, calcium dobesilate

Introduction

Pegylated liposomal doxorubicin (PLD) is widely utilized in treating various cancers due to its outstanding therapeutic efficacy, contributing to enhanced patient survival rates [1]. In comparison to conventional doxorubicin (DOX) drugs, PLD poses a reduced risk of cardiotoxicity, with studies indicating a 3-fold lower incidence of congestive heart failure [2, 3]. However, hand-foot syndrome (HFS), the most prevalent side effect of PLD, can significantly degrade patient quality of life and, in severe cases, necessitate the temporary or permanent discontinuation of treatment [4].

The pathogenesis of PLD-associated HFS remains unclear. Several studies aiming to elucidate the underlying mechanism have posited that HFS is partially triggered by the extravasation of PLD into the skin. Animal models reveal that the skin serves as the primary depot for liposomal drugs [5], and a PLD fluorescence quantitative study in human skin demonstrat ed drug penetration into the stratum corneum and deeper skin layers, leading to HFS [6]. Conventional HFS treatment includes two approaches, supportive care and treatment delay, with or without dosage reduction, however, their efficacy is yet to be substantiated [7]. Therefore, it is essential to explore the underlying complex molecular mechanism and develop novel, effective therapeutic interventions for PLD-induced HFS.

Calcium dobesilate (CaD), a recognized antioxidant and vascular protective agent, has demonstrated decreased blood viscosity and vascular

permeability in patients with diabetic retinopathy [8, 9]. Our previous experiments using rat models and serum samples from breast cancer patients have shown that CaD can mitigate PLD-induced HFS and reduce inflammatory injury in capillary endothelial cells, potentially altering capillary permeability. However, the precise molecular mechanisms underlying PLD-induced HFS and the protective effects of CaD on vascular endothelium remain undefined. Hyaluronic acid (HA), a major component of the extracellular matrix (ECM), has been used as a sensitive marker for exploring endothelial cell function in several studies [10, 11]. Furthermore, it has been reported that HA-CD44 (main receptor for HA) interaction plays an important role in the regulation of low molecular weight HA (LMW-HA, ~200 kD)-induced inflammatory responses [12, 13]. The tight junctions (TJs), one type of intercellular junction [14], play an important role in regulating vascular permeability [15]. Numerous studies have highlighted that the expression of TJ proteins, such as zonula occludens (ZO) and Claudin-5, orchestrates multiple signaling pathways in endothelial cells [14, 16, 17]. Therefore, we hypothesize that HA, CD44, and TJs play an important role in PLD-induced HFS, leading to the preventative action of CaD. The aim of this study is to elucidate these pertinent molecular mechanisms.

Materials and methods

Cell culture and treatment

HMEC-1 cells were obtained from Shanghai Huzhen Industrial Co., Ltd. (Shanghai, China), genotyped using short tandem repeat (STR) analysis, and routinely tested for mycoplasma. These cells were cultured in ECM medium (American Sciencell, CA, USA), supplemented with 5% fetal bovine serum (FBS), 1% streptomycin/penicillin, and 1% endothelial growth factor. Cells were incubated at 37°C in a 5% CO_2 atmosphere with medium changes every two days. Unless otherwise stated, CaD was used to pretreat the cells for 1 hour in cell tests.

Animal housing and establishment of HFS model

Thirty-six female SD rats (6-8 weeks old, 200 g) (Sipeifu [Beijing] Biotechnology Co., Ltd., Beijing, China) were housed with a 12:12 h light-dark cycle, 21±1.5°C, and humidity of 55±15%. The PLD group was intravenously injected with 7 mg/kg PLD (CSPC Ouyi Pharmaceutical Co., Ltd., Shijiazhuang, China) once every 3 days (for 1-10 days). The PLD + CaD group was given 200 mg/kg CaD (MedChemExpress, New Jersey, USA) in 0.5 mL of drinking water daily (for 1-17 days). Rats in the control group were given 0.5 mL of drinking water supplemented with an equivalent dose of PLD. The study was reviewed and approved by Fourth Hospital Ethics Committee of Hebei Medical University. The rats in this study were handled in accordance with the Animal Care and Use Guidelines of the Hebei Medical University (Shijiazhuang, China) under a protocol approved by the Institutional Animal Care and Use.

Transcriptomic analysis

Raw data from RNA-seq were cleaned using fastp software (https://github.com/OpenGene/fastp) to eliminate adaptor contamination, low-quality bases, and undetermined bases using default parameters. Sequence quality was verified using fastp. We employed HISAT2 (https://ccb.jhu.edu/software/hisat2) to map reads to the *Homo sapiens* reference genome. The mapped reads of each sample were assembled using StringTie (https://ccb.jhu.edu/software/stringtie) with default parameters. Then, all transcriptomes from all samples were merged to reconstruct a comprehensive transcriptome using gffcompare (https://github.com/gpertea/gffcompare/). After the final transcriptome was generated, StringTie was used to estimate the expression levels of all transcripts, calculating the expression level for mRNAs via FPKM (FPKM = [total_exon_fragments/mapped_reads (millions) × exon_length (kB)]). Differentially expressed mRNAs were selected using R package edgeR (https://bioconductor.org/packages/release/bioc/html/edgeR.html) with a fold change > 2 or fold change < 0.5 and with parametric F-test comparing nested linear models (p value < 0.05). O function enrichment analysis on gene sets was performed using ClusterProfiler software (R package, v 3.17.0.). GSEA analysis was implemented using log2FoldChange of different genes in descending order.

RNA extraction and real-time quantitative PCR (qPCR)

Total RNA from HMEC-1 cells was extracted and purified using TRIzol reagent (Invitrogen,

Carlsbad, CA, USA) as per the manufacturer's protocol. RNA quantity and purity were assessed using NanoDrop ND-1000 (NanoDrop, Wilmington, DE, USA). Complementary DNA (cDNA) was reverse-transcribed using SuperScript™ II Reverse Transcriptase (Invitrogen, CA, USA). Real-time quantitative PCR was performed using super smart 2× Zapa3g SYBR Green qPCR premix (Zhongshi Gene Technology [Tianjin] Co., Ltd., Tianjin, China). The primers used in the experiment were: HYAL1: forward sequence GACACGACAAACCACTTTCTGCC, reverse sequence ATTTTCCCAGCTCACCCAGAGC; CD44: forward sequence CCAGAAGGAACAGTGGTTTGGC, reverse sequence ACTGTCCTCTGGGCTTGGTGTT; Claudin-5: forward sequence ATGTGGCAGGTGACCGCCTTC, reverse sequence CGAGTCGTACACTTTGCACTGC; ZO-1: forward sequence GTCCAGAATCTCGGAAAAGTGCC, reverse sequence CTTTCAGCGCACCATACCAACC; GAPDH: forward sequence GTCTCCTCTGACTTCAACAGCG, reverse sequence ACCACCCTGTTGCTGTAGCCA.

Western blotting analysis

Protein samples were separated using sodium dodecyl sulfate-polyacrylamide gel electrophoresis and transferred onto a PVDF membrane. Following a 5-minute block with fast blocking solution, the membrane was incubated with target antibodies; specific immunoblotting was performed using ZO-1, CD44, HYAL-1, and Claudin-5 antibodies (all from Wuhan Aibotec Biotechnology Co., Ltd., Wuhan, China) at a 1:1000 dilution, and subsequently with Goat Anti-Rabbit IgG (H+L) HRP antibody at a 1:500 dilution (Affinity, Cincinnati, OH, USA). Images were captured using a Gel imaging system (Fluorchem E, Protein Simple, San Jose, CA, USA), data was normalized to the reference, and expressed as a ratio of target gene expression to reference.

Enzyme-link immunosorbent assay (ELISA) and polyacrylamide gel electrophoresis

The HA content in cell culture medium, serum, and skin homogenates from rat hind paws were quantified by ELISA according to the manufacturer's instructions (CUSABIO, Wuhan, China). Briefly, tissue homogenate was incubated with Protease-E (Solarbio, Beijing, China) at 13 mg/mL at 55°C overnight. Each sample had a control group treated with hyaluronidase (0.2 μg/μL) at 37°C for 1 hour, followed by boiling for 10 minutes. The HA-Ladder (Echelon, Salt Lake City, UT, USA) and corresponding tissue homogenate were subjected to 4-15% polyacrylamide gel electrophoresis. The gel was stained with 0.005% Stains-All (SIGMA-ALDRICH, Missouri, USA) in 50% ethanol for 1 hour and de-stained in 10% ethanol for 10 minutes. Images were captured using the G: BOX XT4 imaging system (Syngene, Cambridge, UK) for analysis. The gray value was determined by subtracting the value of the hyaluronidase-treated matched sample from that of the original sample.

Lactate dehydrogenase (LDH) detection and monolayer cell permeability test

Cells were treated with PLD at a concentration of 10 μg/mL for 1 hour. The presence of LDH in the HMEC-1 culture medium was quantified using the LDH cytotoxicity kit (Beijing Leagene Biotechnology Co., Ltd., Beijing, China). For the monolayer cell permeability test, HMEC-1 cells were seeded in 12-well Transwell inserts (PET, 0.4 μm pore size). Upon cell confluence, the cells were exposed to 10 μg/mL PLD, or 10 μg/mL PLD with 100 μM CaD for 1 hour. FITC-dextran (Ruixibio, Xian, China) (10 kD) was added to each well to achieve a final concentration of 5 mg/mL. After an hour, the ratio of FITC-dextran concentrations was calculated from the outer chamber to the inner chamber.

Cell counting kit-8 (CCK-8)

HMEC-1 cells were seeded on 96-well cell culture plates in 100 μL volumes. Upon reaching 60% confluence, the medium was replaced with medium containing varying concentrations of PLD (0.125 μg/mL, 0.25 μg/mL, 0.5 μg/mL, 1 μg/mL, 2 μg/mL, 4 μg/mL, 6 μg/mL, 8 μg/mL, 10 μg/mL) while maintaining a control group. After the addition of 10 μL of CCK-8 reagents (Hebei Report Biotechnology Co., Ltd., Shijiazhuang, China) to each well, plates were incubated for 2 hours at 37°C in the dark. Optical density (OD) was measured at 450 nm using a microplate reader (Bio-Tek, Winooski, VT, USA).

Quantification of vascular leakage and PLD in rat paw skin

After anesthetizing rats with inhalants, 1 mL/kg of Evans Blue solution (Shanghai Macklin

Biochemical Technology Co., Ltd., Shanghai, China) was injected into the tail vein. Evans Blue absorbance was measured at 610 nm using a microplate reader. Extracted dye was calculated by extrapolation from a standard curve of varying Evans Blue solution concentrations. Rats were subsequently euthanized, perfused with heparin saline, and back paw skin tissues were collected, weighed, and stored at -80°C for subsequent analysis against the standard curve.

Immunofluorescence and hematoxylin-eosin (H&E) staining

HMEC-1 cells were fixed with 4% PFA for 15 min and blocked with 2% BSA at room temperature for 1 h. Primary antibodies (Wuhan Aibotec Biotechnology Co., Ltd., Wuhan, China) at a 1:50 dilution were added to the blocking buffer and incubated overnight at 4°C. Secondary antibodies (1:500 dilution) (Seracare, Milford, MA, USA) were then added and incubated for 1 hour at room temperature. Slides were prepared using Prolong Gold Antifade Reagent with DAPI (Hebei Report Biotechnology Co., Ltd., Shijiazhuang, China), and images captured with a laser confocal microscope (LSM 900 Carl Zeiss, Jena, Germany). Hind paw skin tissues were harvested, fixed, and dehydrated with ethanol and embedded in paraffin. After 24 h, the tissue was embedded in paraffin, sectioned, stained with H&E, and sealed with neutral resin. The pathological changes were observed under an optical microscope.

Scanning electron microscopy

Thin tissue sections were sliced with an ultramicrotome, washed, stained, dehydrated, and finally embedded in EPON (liquid epoxy) resin. Imaging was conducted using a transmission electron microscope (HT7800, Hitachi, Japan).

Statistical analysis

Statistical analysis was performed using SPSS 23.0 software (SPSS Inc., Chicago, IL, USA). Data are presented as mean ± standard deviation. Differences between treatments were evaluated using Student's t-test. Multi-group comparisons were made conducted using analysis of variance (ANOVA), followed by an LSD test for between-group comparison. A p-value < 0.05 was considered significant.

Results

ECM and TJ pathway enrichment after PLD intervention

To investigate the mechanism of PLD damage on endothelial cells, we selected 0.25 μg/mL PLD (72 h cell survival rate was 83.03%±1.59%) to treat HMEC-1 cells for 72 h. Untreated HMEC-1 cells were used as a control group. Expression cut-off values of log (fold-change) > 1.0 or < -1.0 and p-value < 0.05 revealed 2187 differentially expressed genes (DEGs), which comprised 1180 upregulated and 1007 downregulated genes. Gene ontology (GO) enrichment showed that the 34 DEGs were mainly involved the extracellular region, ECM, plasma membrane receptor complex, an anchored component of the external side plasma membrane, and integral components of the plasma membrane in cellular components (**Figure 1A**), and 11 DEGs were mainly involved extracellular structural organization, positive regulation of endothelial cell proliferation, and positive regulation of vascular endothelial cell proliferation in biological process (**Figure 1B**). GSEA pathway analysis was performed to further elucidate the biological processes of PLD damage on endothelial cells. GSEA analysis showed an enrichment in differentially expressed genes involved in TJs (**Figure 1C**). Informed by the enrichment pathway analysis, we used qPCR and western blot to analyze the expression of HA-degrading enzyme hyaluronidase (HYAL)-1 and its receptor CD44, as well as TJs-associated proteins Claudin-5 and ZO-1. We found that PLD treatment up-regulated the expression of HYAL-1 and CD44, and down-regulated the expression of Claudin-5 and ZO-1 (P < 0.05; **Figure 1D** and **1E**).

CaD partially alleviates PLD-induced degradation of HA and the downregulation of TJs

To further understand the specific mechanism of PLD affecting TJs protein, we examined the roles of HYAL and CD44. Initial treatment with 50 μg/mL hyaluronidase showed a corresponding increase in CD44 expression and a decrease in Claudin-5 and ZO-1 while HYAL-1 remained unchained (P < 0.05; **Figure 2A**).

Next, we examined the effects of a 1 hour, 1 nM AD-01 (CD44 inhibitor) pretreatment prior to PLD incubation (0.25 ug/ml). This was com-

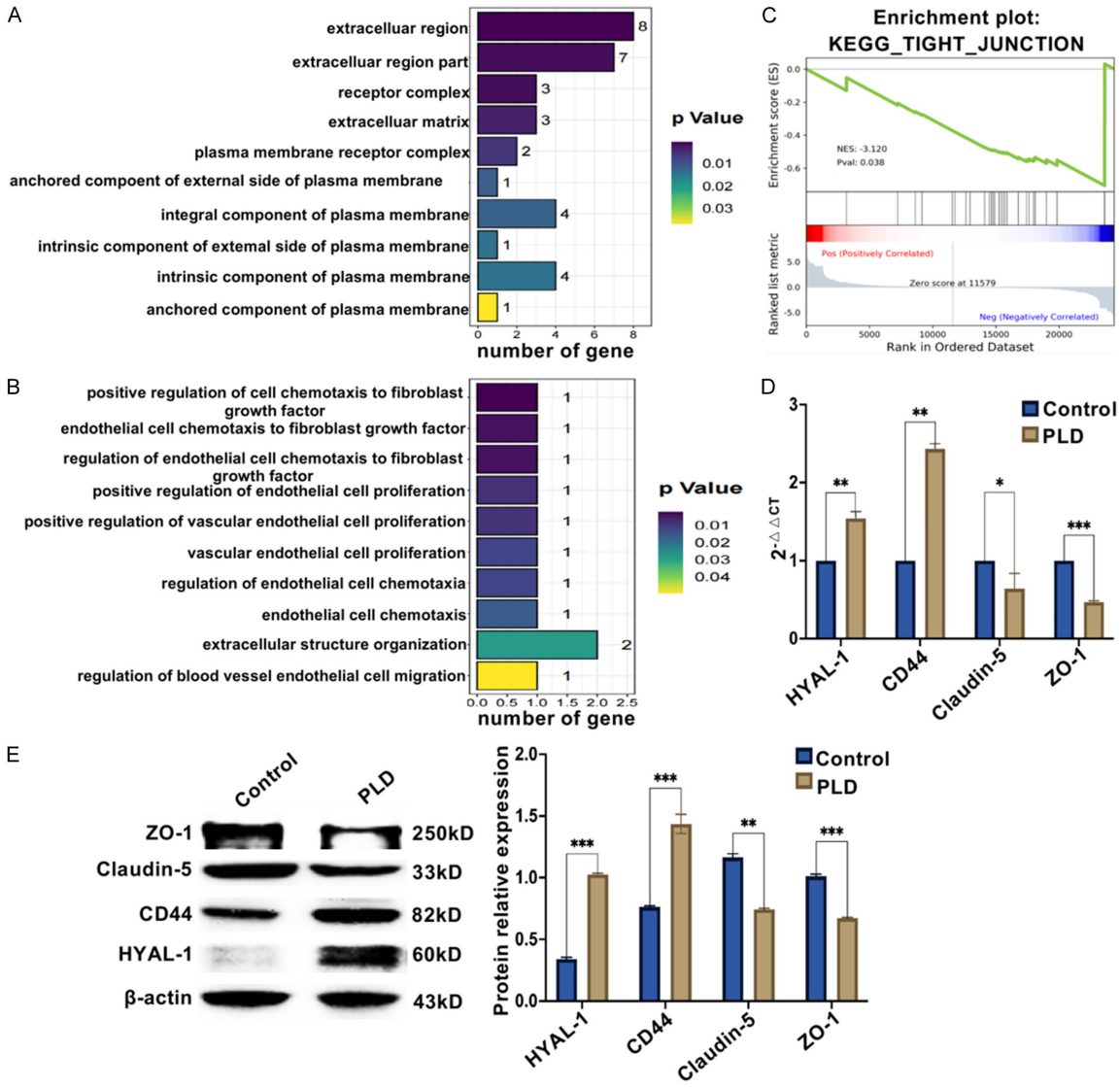

Figure 1. After PLD intervention, the potential pathways were enriched in ECM and TJs, the expression of HYAL-1 and CD44 were up-regulated, and TJs were down-regulated. A: Analysis of cell components after PLD intervention in HMEC-1; B: Analysis of biological processes after PLD intervention in HMEC-1; C: GSEA analysis of tight junction in HMEC-1; D: Relative gene expression levels of HYAL-1, CD44, Claudin-5, and ZO-1 after PLD intervention in HMEC-1 by qPCR (n=3, $*P < 0.05$, $**P < 0.01$, $***P < 0.001$); E: Expression levels of HYAL-1, CD44, Claudin-5, and ZO-1 after PLD intervention in HEMEC-1 by western Blot (n=3, $**P < 0.01$, $***P < 0.001$).

pared to PLD-only and control groups. Expression of Claudin-5 and ZO-1 in the PLD + AD-01 group was higher than that in the PLD group after 72 hours ($P < 0.05$; **Figure 2B**). We further conducted experiments of PLD combined with or without 100 μM CaD intervention in vitro and in vivo to explore the CaD function. The qPCR and western blot results in HMEC-1 cells found that CaD could partially reverse elevated of HYAL-1 and CD44 levels while reducing of the expression of Claudin-5 and ZO-1 caused by PLD ($P < 0.05$; **Figure 2C** and **2D**). The hind paw skin tissue displayed similar outcomes (**Figure 2E**), confirming that CaD partially mitigates PLD-induced HA degradation and down-regulation of TJs.

CaD inhibits PLD-induced degradation of HA

We measured HA levels in the cell culture medium, rat serum, and skin tissue to assess the metabolic impact of PLD and CaD. ELISA results indicated no significant difference in HA levels in the culture supernatants of the control, PLD

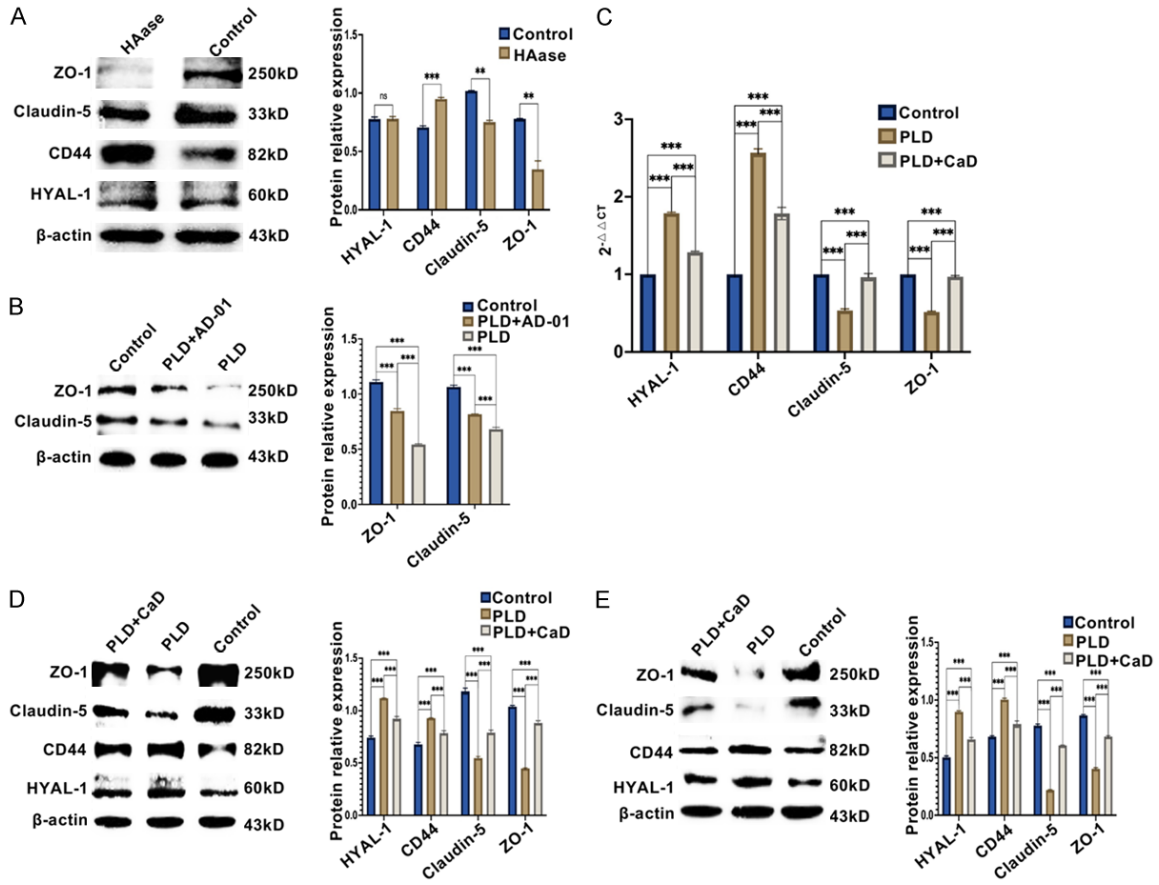

Figure 2. CaD reduced the expression of HYAL-1 and alleviated the down-regulation of TJs caused by PLD via the HA/CD44 signaling pathway. A: Effect of hyaluronidase on the expression of HYAL-1, CD44, Claudin-5, and ZO-1 in HMEC-1 by western blot (n=3, ns, Non-significant, $^{**}P < 0.01$, $^{***}P < 0.001$); B: Effect of PLD with or without CD44 inhibitor (AD-01) on the expression of Claudin-5 and ZO-1 in HMEC-1 by western blot (n=3, $^{***}P < 0.001$); C: Effect of PLD combined with or without CaD on the expression of HYAL-1, CD44, Claudin-5, and ZO-1 in HMEC-1 by qPCR (n=3, $^{***}P < 0.001$); D: Effect of PLD combined with or without CaD on the expression of HYAL-1, CD44, Claudin-5, and ZO-1 in HMEC-1 by western blot (n=3, $^{***}P < 0.001$); E: Effect of PLD combined with or without CaD on the expression of HYAL-1, CD44, Claudin-5, and ZO-1 in skin tissue of rat hind paw by western blot (n=3, $^{***}P < 0.001$).

(0.25 ug/ml), and PLD (0.25 ug/ml) + CaD (100 uM) groups ($P > 0.05$; **Figure 3A**). However, PLD treatment significantly increased the HA level in rat serum, while CaD partially reversed this effect ($P < 0.05$; **Figure 3B**). Polypropylene gel electrophoresis revealed PLD treatment was significantly associated with the degradation of HA with a molecular greater than 480 kD compared with the control group ($P < 0.05$). This degradation was significantly associated with increased levels of HA with a molecular weight range of 74-198 kD, 198-498 kD, and 32-74 kD; this was partially reversed by CaD ($P < 0.05$; **Figure 3C**). These findings suggest that PLD degrades HA and increases serum HA levels, whereas CaD inhibits excessive PLD-induced HA degradation. However, the unaltered HA secretion implies PLD may not affect HA synthesis.

CaD mitigates PLD-induced endothelial permeability in vitro and in vivo

To elucidate the mechanisms underlying PLD extravasation and the protective effect of CaD on Tight Junctions (TJs), we evaluated the impact of PLD on endothelial permeability both in vitro and in vivo, and assessed the expression of TJs. Initially, cells were seeded in 96-well plates, followed by treatment with PLD for 1 h to measure lactate dehydrogenase. We observed that 10 μg/mL PLD exposure for 1 h did not significantly elevate lactate dehydrogenase levels ($P > 0.05$; **Figure 4A**), thereby elimi-

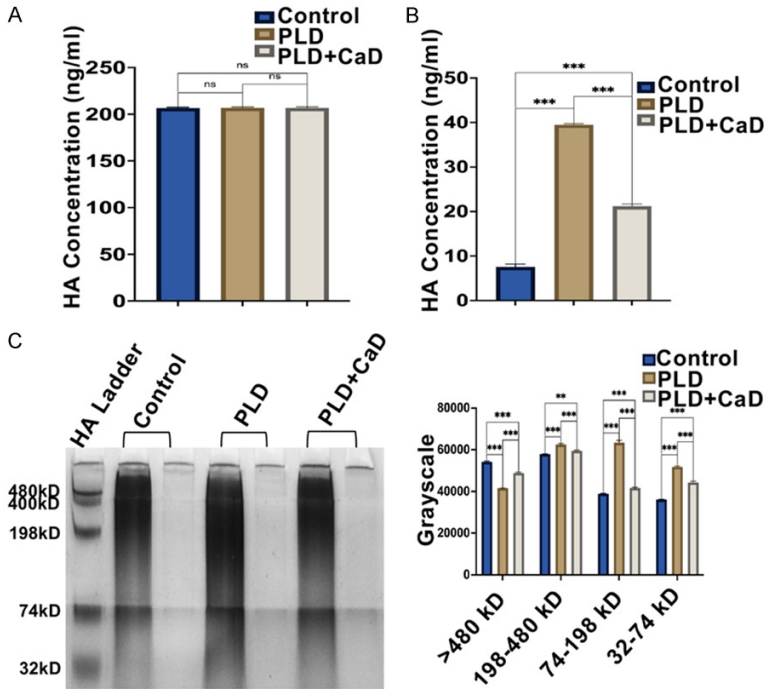

Figure 3. CaD reduced the degradation of HA caused by PLD. A: HA concentration in cell culture medium detected by ELISA (n=3, ns, Non-significant); B: HA concentration in rat serum detected by ELISA (n=3, ***$P < 0.001$); C: The molecular weight distribution of HA in rat hind paw tissue homogenate by polypropylene gel electrophoresis (n=3, **$P < 0.01$, ***$P < 0.001$).

nating potential cytotoxicity effects on permeability. Subsequently, cells were seeded onto 12-well Transwell inserts with a pore size of 0.4 μm. Following cell confluence, cells were treated with 10 μg/ml PLD, with or without 100 μM CaD for 1 h, alongside a control group. The Optical Density (OD) values of FITC-dextran in the inner and outer chambers were measured independently, and the ratio of the OD value in the outer chamber to the inner chamber was analyzed. Leakage of FITC-dextran into the external chamber was significantly higher in the PLD group compared with the control group, while CaD notably mitigated PLD-induced FITC-dextran extravasation ($P < 0.05$; **Figure 4B**). Moreover, immunofluorescence assays revealed decreased Claudin-5 and ZO-1 expression in the PLD group relative to the control group, whereas CaD treatment partly alleviated this downregulation ($P < 0.05$; **Figure 4E**). We used Evans blue to detect the permeability of rat hind paw skin capillaries in vivo. Results were consistent with in vitro experiments (**Figure 4C**). Furthermore, we determined drug concentrations in rat hindfoot skin tissue and found that the DOX concentration in the PLD group was significantly higher than those in the PLD + CaD group ($P < 0.05$; **Figure 4D**). Collectively, these results indicate that PLD enhances capillary permeability by reducing TJ-associated protein expression, thereby promoting PLD extravasation whereas CaD can partially counteract these effects.

CaD alleviates PLD-induced capillary and skin tissue damage and prevents severe HFS

To further investigate the deleterious impact of PLD on capillaries and skin tissue, as well as the preventive role of CaD on HFS in animal models, we qualitatively analyzed the incidence of HFS and changes in TJ expression of capillary endothelial cells in animal models. We established a PLD-induced HFS model via intravenous administration of 7 mg/kg PLD to female SD rats. Observations began 10 days post-PLD administration. In the PLD group, rat hind paws exhibited symptoms of erythema, swelling, and ulceration (**Figure 5A**). Ignoring the mortality rate during the experiment, we noted 7 instances of grade III HFS (85.71%) and 1 instance of grade I-II HFS in the PLD group. There were no grade III HFS cases and 9 instances of grade I-II HFS in the PLD + CaD group. Hematoxylin and eosin (HE) staining of the rat hind paw skin tissue revealed epidermal layer alterations (almost complete disappearance of the clear and granular layers, swollen and thickened spinous layer, disordered basal layer), reduced epidermal fibers with disorganized and sparse cells, and loss of cell polarity following PLD treatment. In addition, dermal endothelial cell count decreased, arrangement was sparse, cell volume shrank, and blood vessels appeared dilated (**Figure 5B**). Finally, the skin capillary was observed by transmission electron microscope. The result showed that cell division, vesicles increased, basement membrane separation, peripheral edema, and opening of TJs in capillary endothelial cells after PLD intervention (**Figure 5C**). Notably, the CaD

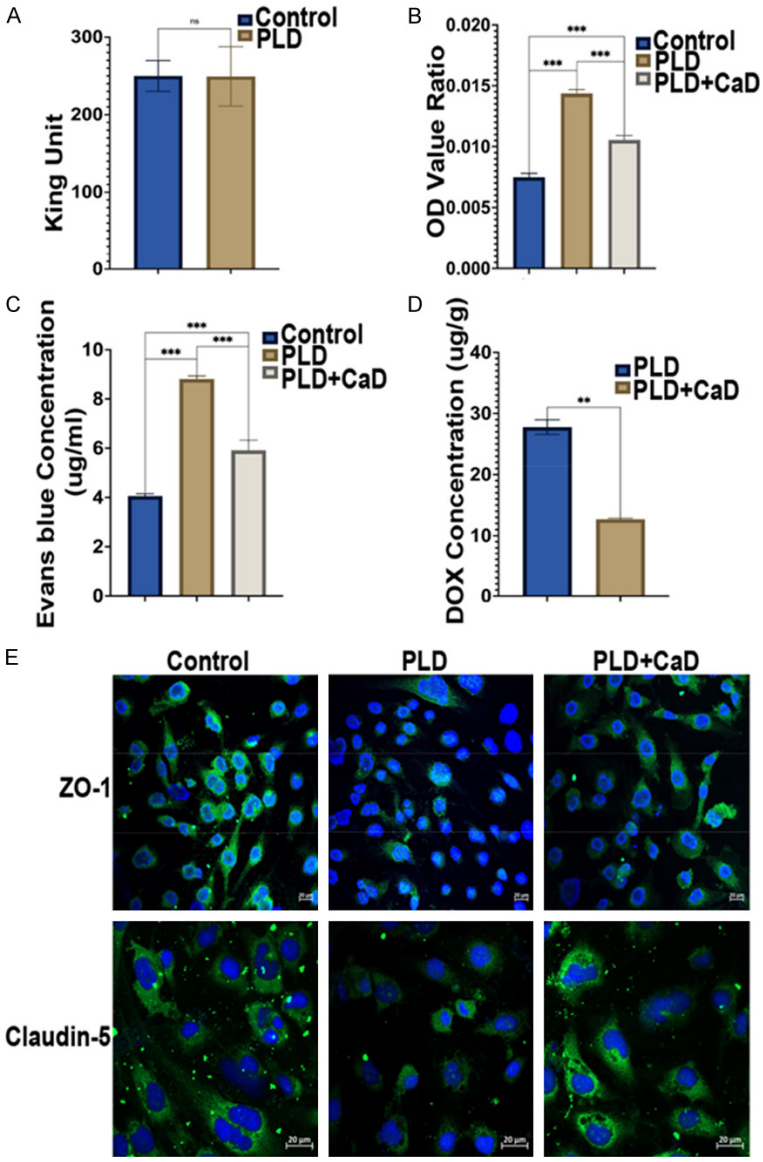

Figure 4. CaD alleviated PLD-induced endothelial permeability in vitro and in vivo. A: After PLD treatment of HMEC-1, the LDH activity of cells was detected by colorimetry (n=3, ns, Non-significant); B: FITC-dextran was used to detect the permeability of monolayer cells. The ratio of OD in the outer chamber to OD within the insert was quantified (n=3, ***P < 0.001); C: The change of skin capillary permeability was judged by detecting the concentration of Evans blue in the skin tissue of hind paw of rats (n=3, ***P < 0.001); D: Effect of PLD combined with or without CaD on DOX concentration in rat hind paw skin tissue (n=3, **P < 0.01); E: Expression of Claudin-5 and ZO-1 by immunofluorescence. Scale bars =20 μM. Claudin-5 and ZO-1 are labeled green with the nucleus counterstained in blue.

treatment group exhibited improvement in all symptoms. The morphological findings suggest that PLD-induced HFS is due to TJ damage leading to exudation, and that CaD can both ameliorate these changes and prevent the development of severe HFS.

Discussion

PLD is a representative nanomedicine approved for the treatment of various cancers with promising therapeutic efficacy [18]. However, HFS, a well-established cutaneous adverse event of PLD, has severe impacts on patient treatment by hindering daily activities, reducing compliance, and negatively affecting quality of life [19]. Moreover, due to the poorly understood pathogenesis of HFS, no effective treatment has been identified [20]. Consequently, insights into the molecular mechanisms underlying PLD-induced HFS and potential treatment strategies are essential.

In this study, we initially explored the differentially expressed genes of cellular components and biological processes through GO and GSEA analysis. We found that the discrepancies were enriched in the extracellular matrix, plasma membrane components, and TJs. Given that HA and members of the HA family, such as HYAL-1 hyaluronidase and CD44, are highly abundant in skin tissue and serve diverse biological roles in various diseases [21, 22], we sought to investigate the roles of HA and TJs in PLD-induced HFS. We examined the expression of HYAL-1, CD44, and TJ proteins (Claudin-5 and ZO-1). We found that PLD upregulates the expression of HYAL-1 and CD44 while downregulating the expression of Claudin-5 and ZO-1. These findings suggest that our selected indicators may contribute to the pathogenesis of HFS. Recent studies have reported that HA influences the blood-brain barrier through a CD44-dependent pathway

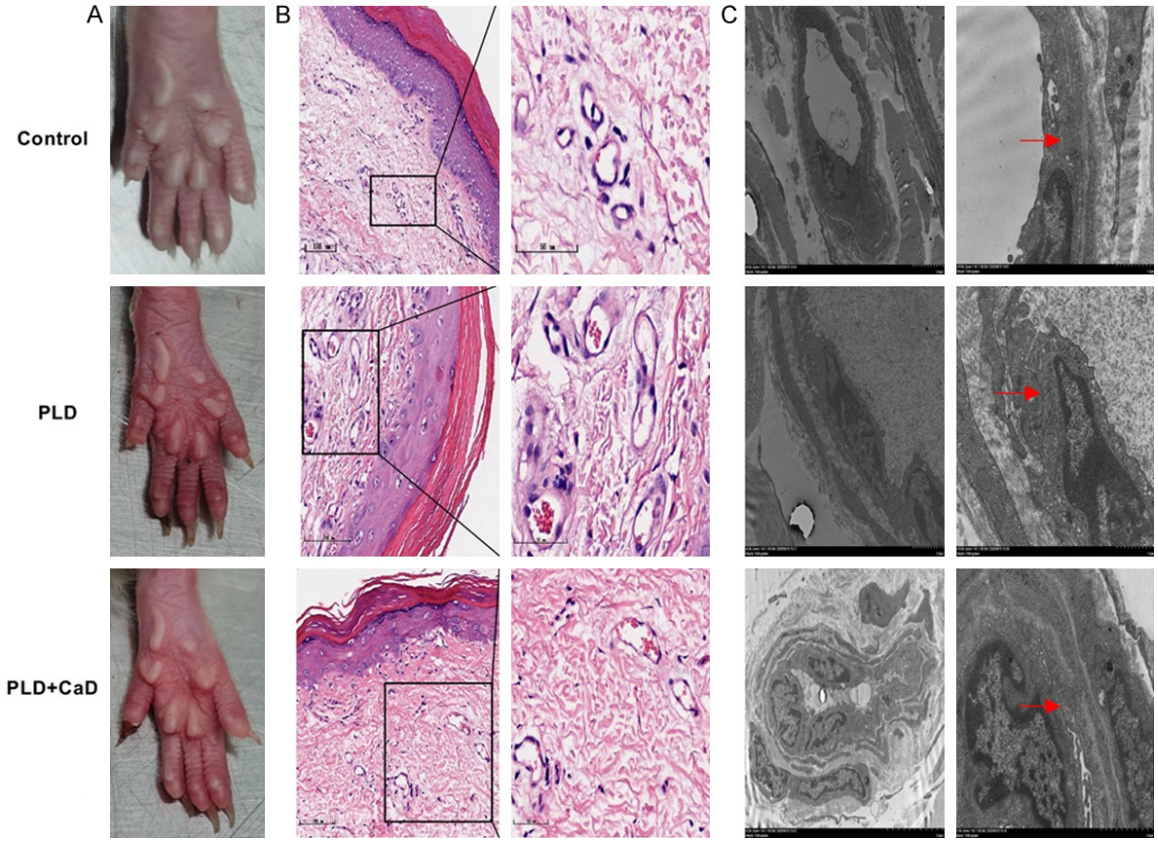

Figure 5. CaD reduced the damage of PLD to capillaries and skin tissues, preventing the occurrence of severe HFS. A: Observation rat hind paw lesions after PLD and CaD intervention; B: HE staining of rat hind paw skin tissue. Scale bars 100 μM (left column) and 50 um (right column); C: Observation of capillaries and endothelial cells in rat hind paw skin tissue by transmission electron microscope. The red arrow indicates the tight junction.

and may be associated with decreased TJs protein levels [23]. Another study also revealed that HA could affect CD44 and tight junction protein expression [24]. Our study aligns with these findings; after employing AD-01 (an inhibitor of CD44 [25]), we noted that PLD-driven decreases in Claudin-5 and ZO-1 expression were mitigated. This suggests PLD influences HA and TJ function via a CD44-dependent pathway.

Subsequently, we further examined the specific functions of HA and TJs in PLD intervention. Choi et al. reported that PLD accumulates effectively in tumor tissue due to the degradation of the HA backbone [26], which is consistent with our study. Our investigations into HA metabolism revealed that changes in the expression of CD44, Claudin-5, and ZO-1 did not directly regulate HYAL-1 expression level, but impacted HA degradation. We also directly observed a decrease in high molecular weight HA and an increase in low molecular weight HA after PLD intervention using polyacrylamide gel electrophoresis. Studies have shown that the distribution of Doxil in tumors might be influenced by vascular permeability [27, 28]. Our study confirmed that PLD enhances capillary permeability, as evidenced by experimental studies of monolayer HMEC-1 and rat hind paw skin capillaries in both quantitative and qualitative tests. Concurrently, we observed an increase in DOX concentration. This could be one reason for the increase in PLD extravasation, leading to enhanced skin tissue accumulation of PLD and subsequent HFS. Our findings align with a recent study by Huang et al., who found that drug delivery of the Dox complex in tumor cells correlated with HA degradation and HA-CD44 binding [29].

Our previous research has shown that CaD can prevent PLD-induced HFS [30], and CaD (as a vascular protection drug) has the ability to

reduces vascular permeability [31]. Thus, we investigated the protective mechanism of CaD on blood vessels and its therapeutic effect on HFS. We found that CaD counteracted PLD-induced changes in the four aforementioned indices, HYAL-1, CD44, Claudin-5, and ZO-1 levels, reduced HA degradation, and further decreased vascular permeability. This is consistent with several studies. Leal et al. reported that CaD decreased blood viscosity and retinal vessel microvascular hyperpermeability [32] and altered the distribution of Claudin-5 and ZO-1 in TJs [33]. Moreover, we note that CaD reduced the progression of pathological lesions in the kidney [34], a finding we also observed in our study. Staining and electron microscopy revealed CaD improved pathological lesions in the skin of rat hind paws, with notable changes in the granular layer and spinous layer. This study marks the first time we have identified a novel target pathway for CaD-regulated vascular permeability by inhibiting HYAL-1. Given that the HA content in the dermis is five times that of the epidermis, while HYAL-1 is mostly expressed in the granular and spinous layers of the epidermis [35], our findings suggest that histological features, HA content, and basal HYAL-1 expression levels are factors in predicting HFS risk.

It should be noted that our research has certain limitations. First, besides hyaluronidase, other HA degradation pathways such as reactive oxygen species (ROS) exist, and ROS has been suggested to be the cause of HFS. Furthermore, CaD can inhibit ROS production [36, 37], suggesting that, besides HYAL-1, other factors could contribute to HA degradation in PLD-induced HFS tissue and CaD's vascular protective effects. Second, HA in the skin has roles in regulating keratin-forming cell proliferation and differentiation, participating in epidermal barrier function, and modulating inflammatory responses [38, 39]. Therefore, besides regulating TJs proteins, changes in HA concentration and molecular weight might also play a significant role in HFS pathogenesis, and the specific mechanisms warrant further investigation. Third, while this study and previous conclusions suggest that low molecular weight HA can affect TJ protein expression via CD44, the specific molecular weight fragment for the CD44 receptor remains unclear. Fourth, this study lacked a correlation analysis between serum HA concentration and HFS levels in rats, and our study of HA molecular weight distribution was unsuccessful due to low HA content in the cell culture medium. Fifth, our experiment lacks research on these important indexes in human specimens. We are actively collecting blood and skin samples from patients' hands and feet, as well as clinical data on the protective effect of CaD on HFS. It is our belief that the results of this study can be validated by clinical trials and then popularized.

Conclusions

In summary, our research elucidates a potential mechanism underpinning PLD-induced HFS. We propose that PLD may disrupt TJs through the HA/CD44 pathway, leading to increased skin permeability and intensified doxorubicin extravasation, thus contributing to HFS. Simultaneously, CaD appears to inhibit this signaling pathway, thereby improving vascular permeability, reducing tissue drug accumulation, and alleviating HFS symptoms. Our findings thus offer insight into potential mechanisms of PLD-induced HFS and illuminate novel therapeutic approaches for HFS. Driven by these findings, we are presently conducting clinical trials to validate the protective effects of CaD on HFS, and we anticipate promising results.

Acknowledgements

This study is supported by Hebei Province Natural Science Foundation (H2020206365, H2021206071), Bethune Basic Research Program on Cancer (BCF-NH-ZL-20201119-013) and the Wu Jieping Medical Foundation for Clinical Scientific Research (320.6750.13295). The funding body had no role in the design or execution of the study.

Disclosure of conflict of interest

None.

Address correspondence to: Zhen-Chuan Song, Department of Breast Center, The Fourth Hospital of Hebei Medical University, Shijiazhuang 050000, Hebei, P. R. China. ORCID: 0000-0003-3674-1946; E-mail: songzhch@hotmail.com

References

[1] Yang J, Qiao L, Zeng Z, Wang J, Zhu T, Wei J, Wu M, Ye S, Huang X, Ma D, Liu R and Gao Q. The

role of the ATM/Chk/P53 pathway in mediating DNA damage in hand-foot syndrome induced by PLD. Toxicol Lett 2017; 265: 131-139.
[2] Gabizon AA, Patil Y and La-Beck NM. New insights and evolving role of pegylated liposomal doxorubicin in cancer therapy. Drug Resist Updat 2016; 29: 90-106.
[3] You S, Zuo L and Li W. Optimizing the time of Doxil injection to increase the drug retention in transplanted murine mammary tumors. Int J Nanomedicine 2010; 5: 221-229.
[4] Yokomichi N, Nagasawa T, Coler-Reilly A, Suzuki H, Kubota Y, Yoshioka R, Tozawa A, Suzuki N and Yamaguchi Y. Pathogenesis of hand-foot syndrome induced by PEG-modified liposomal doxorubicin. Hum Cell 2013; 26: 8-18.
[5] Gabizon A, Goren D, Horowitz AT, Tzemach D, Lossos A and Siegal T. Long-circulating liposomes for drug delivery in cancer therapy: a review of biodistribution studies in tumor-bearing animals. Adv Drug Deliv Rev 1997; 24: 337-344.
[6] Lademann J, Martschick A, Jacobi U, Richter H, Darvin M, Sehouli J, Oskay-Oezcelik G, Blohmer JU, Lichtenegger W and Sterry W. Investigation of doxorubicin on the skin: a spectroscopic study to understand the pathogenesis of PPE. J Clin Oncol 2005; 23: 5093-5093.
[7] von Moos R, Thuerlimann BJ, Aapro M, Rayson D, Harrold K, Sehouli J, Scotte F, Lorusso D, Dummer R, Lacouture ME, Lademann J and Hauschild A. Pegylated liposomal doxorubicin-associated hand-foot syndrome: recommendations of an international panel of experts. Eur J Cancer 2008; 44: 781-790.
[8] Haller H, Ji L, Stahl K, Bertram A and Menne J. Molecular mechanisms and treatment strategies in diabetic nephropathy: new avenues for calcium dobesilate-free radical scavenger and growth factor inhibition. Biomed Res Int 2017; 2017: 1909258.
[9] Liu J, Li S and Sun D. Calcium dobesilate and micro-vascular diseases. Life Sci 2019; 221: 348-353.
[10] Suehiro T, Boros P, Emre S, Sheiner P, Guy S, Schwartz ME and Miller CM. Assessment of liver allograft function by hyaluronic acid and endothelin levels. J Surg Res 1997; 73: 123-128.
[11] Williams AM, Langley PG, Osei-Hwediah J, Wendon JA and Hughes RD. Hyaluronic acid and endothelial damage due to paracetamol-induced hepatotoxicity. Liver Int 2003; 23: 110-115.
[12] Collins SL, Black KE, Chan-Li Y, Ahn YH, Cole PA, Powell JD and Horton MR. Hyaluronan fragments promote inflammation by down-regulating the anti-inflammatory A2a receptor. Am J Respir Cell Mol Biol 2011; 45: 675-683.
[13] Misra S, Hascall VC, Markwald RR and Ghatak S. Interactions between hyaluronan and its receptors (CD44, RHAMM) regulate the activities of inflammation and cancer. Front Immunol 2015; 6: 201.
[14] Wallez Y and Huber P. Endothelial adherens and tight junctions in vascular homeostasis, inflammation and angiogenesis. Biochim Biophys Acta 2008; 1778: 794-809.
[15] Pulous FE and Petrich BG. Integrin-dependent regulation of the endothelial barrier. Tissue Barriers 2019; 7: 1685844.
[16] Hwang SR and Kim K. Nano-enabled delivery systems across the blood-brain barrier. Arch Pharm Res 2014; 37: 24-30.
[17] Kook SY, Hong HS, Moon M, Ha CM, Chang S and Mook-Jung I. Aβ1-42-RAGE interaction disrupts tight junctions of the blood-brain barrier via Ca2+-calcineurin signaling. J Neurosci 2012; 32: 8845-8854.
[18] O'Shaughnessy JA. Pegylated liposomal doxorubicin in the treatment of breast cancer. Clin Breast Cancer 2003; 4: 318-328.
[19] Nikolaou V, Syrigos K and Saif MW. Incidence and implications of chemotherapy related hand-foot syndrome. Expert Opin Drug Saf 2016; 15: 1625-1633.
[20] Kang YK, Lee SS, Yoon DH, Lee SY, Chun YJ, Kim MS, Ryu MH, Chang HM, Lee JL and Kim TW. Pyridoxine is not effective to prevent hand-foot syndrome associated with capecitabine therapy: results of a randomized, double-blind, placebo-controlled study. J Clin Oncol 2010; 28: 3824-3829.
[21] Zhang X, Sun D, Song JW, Zullo J, Lipphardt M, Coneh-Gould L and Goligorsky MS. Endothelial cell dysfunction and glycocalyx - a vicious circle. Matrix Biol 2018; 71-72: 421-431.
[22] Kramer MW, Escudero DO, Lokeshwar SD, Golshani R, Ekwenna OO, Acosta K, Merseburger AS, Soloway M and Lokeshwar VB. Association of hyaluronic acid family members (HAS1, HAS2, and HYAL-1) with bladder cancer diagnosis and prognosis. Cancer 2011; 117: 1197-1209.
[23] Al-Ahmad AJ, Patel R, Palecek SP and Shusta EV. Hyaluronan impairs the barrier integrity of brain microvascular endothelial cells through a CD44-dependent pathway. J Cereb Blood Flow Metab 2019; 39: 1759-1775.
[24] Rooney P, Srivastava A, Watson L, Quinlan LR and Pandit A. Hyaluronic acid decreases IL-6 and IL-8 secretion and permeability in an inflammatory model of interstitial cystitis. Acta Biomater 2015; 19: 66-75.
[25] Yaghobi Z, Movassaghpour A, Talebi M, Abdoli Shadbad M, Hajiasgharzadeh K, Pourvahdani

S and Baradaran B. The role of CD44 in cancer chemoresistance: a concise review. Eur J Pharmacol 2021; 903: 174147.
[26] Choi KY, Min KH, Yoon HY, Kim K, Park JH, Kwon IC, Choi K and Jeong SY. PEGylation of hyaluronic acid nanoparticles improves tumor targetability in vivo. Biomaterials 2011; 32: 1880-1889.
[27] Song G, Wu H, Yoshino K and Zamboni WC. Factors affecting the pharmacokinetics and pharmacodynamics of liposomal drugs. J Liposome Res 2012; 22: 177-192.
[28] Carvalho C, Santos RX, Cardoso S, Correia S, Oliveira PJ, Santos MS and Moreira PI. Doxorubicin: the good, the bad and the ugly effect. Curr Med Chem 2009; 16: 3267-3285.
[29] Huang Y, Song C, Li H, Zhang R, Jiang R, Liu X, Zhang G, Fan Q, Wang L and Huang W. Cationic conjugated polymer/hyaluronan-doxorubicin complex for sensitive fluorescence detection of hyaluronidase and tumor-targeting drug delivery and imaging. ACS Appl Mater Interfaces 2015; 7: 21529-21537.
[30] Song Z, Tian F, Feng S, Shi L, Chen X, Liu X, Wang M, Qi Y, Hui T and Fu Y. Pegylated liposomal doxorubicin-induced hand-foot syndrome predicted by serum metabolomic profiling and prevented by calcium dobesilate. J Am Acad Dermatol 2022; 86: 688-690.
[31] Mahi-Birjand M, Yaghoubi S, Abdollahpour-Alitappeh M, Keshtkaran Z, Bagheri N, Pirouzi A, Khatami M, Sineh Sepehr K, Peymani P and Karimzadeh I. Protective effects of pharmacological agents against aminoglycoside-induced nephrotoxicity: a systematic review. Expert Opin Drug Saf 2020; 19: 167-186.
[32] Leal EC, Santiago AR and Ambrosio AF. Old and new drug targets in diabetic retinopathy: from biochemical changes to inflammation and neurodegeneration. Curr Drug Targets CNS Neurol Disord 2005; 4: 421-434.
[33] Leal EC, Martins J, Voabil P, Liberal J, Chiavaroli C, Bauer J, Cunha-Vaz J and Ambrosio AF. Calcium dobesilate inhibits the alterations in tight junction proteins and leukocyte adhesion to retinal endothelial cells induced by diabetes. Diabetes 2010; 59: 2637-2645.
[34] Bazmandegan G, Fatemi I, Kaeidi A, Khademalhosseini M, Fathinejad A and Amirteimoury M. Calcium dobesilate prevents cisplatin-induced nephrotoxicity by modulating oxidative and histopathological changes in mice. Naunyn Schmiedebergs Arch Pharmacol 2021; 394: 515-521.
[35] Zadnikova P, Sinova R, Pavlik V, Simek M, Safrankova B, Hermannova M, Nesporova K and Velebny V. The degradation of hyaluronan in the skin. Biomolecules 2022; 12: 251.
[36] Garantziotis S and Savani RC. Hyaluronan biology: a complex balancing act of structure, function, location and context. Matrix Biol 2019; 78-79: 1-10.
[37] Njau F and Haller H. Calcium dobesilate modulates PKCdelta-NADPH oxidase-MAPK-NF-kappaB signaling pathway to reduce CD14, TLR4, and MMP9 expression during monocyte-to-macrophage differentiation: potential therapeutic implications for atherosclerosis. Antioxidants (Basel) 2021; 10: 1798.
[38] Evrard C, Lambert de Rouvroit C and Poumay Y. Epidermal hyaluronan in barrier alteration-related disease. Cells 2021; 10: 3096.
[39] Hauser-Kawaguchi A, Luyt LG and Turley E. Design of peptide mimetics to block pro-inflammatory functions of HA fragments. Matrix Biol 2019; 78-79: 346-356.